Heliyon 9 (2023) e20871

Contents lists available at ScienceDirect

Heliyon

journal homepage: www.cell.com/heliyon

Effect of stabilizer content in different solvents on the synthesis of ZnO nanoparticles using the chemical precipitation method

M. Ummay Sumaya [a], Kazi Hanium Maria [a,*], F.T.Z. Toma [b], M.A. Zubair [c], M.T. Chowdhury [d]

[a] Department of Physics, University of Dhaka, Bangladesh
[b] Experimental Physics Division, Atomic Energy Centre, Dhaka-1000, Bangladesh
[c] Department of Nanomaterials and Ceramic Engineering, Bangladesh University of Engineering and Technology (BUET), Dhaka-1000, Bangladesh
[d] Institute of Energy Science, Atomic Energy Research Establishment, Bangladesh Atomic Energy Commission, P.O Box 3787, Dhaka-1000, Bangladesh

ARTICLE INFO

Keywords:
ZnO NPs
Chemical precipitation method
Stabilizer
Optical properties
Crystallite size

ABSTRACT

Zinc Oxide (ZnO) nanoparticles (NPs) have been synthesized by a simple chemical precipitation method. The effect of monoethanolamine (MEA) content in different solvents on ZnO NPs synthesis and their structural properties has been investigated. The NPs synthesized by using isopropanol (IPA) with 15 ml MEA as a stabilizer under the most favorable conditions (deposition time, t_d = 120 min, temperature = 60 °C) showed good structural properties. Synthesized NPs exhibited beneficial structural properties after annealing. The hexagonal wurtzite crystal structure of ZnO NPs was verified by XRD. Different models were used to calculate structural parameters such as crystallite size, strain, stress, and energy density for all the reflection peaks of XRD corresponding to ZnO lying in the range 2θ = 15°–80°. The crystallite size of the ZnO nanoparticles was found to be 50–60 nm. FTIR and EDX confirmed the presence of ZnO NPs in the samples. SEM micrograph of all the samples revealed that the grain sizes decrease gradually with the increase of the amount of MEA. UV–Visible diffuse reflectance spectroscopy results provide evidence that the ZnO NPs possess broader absorption bands, together with high band gap energy. The ZnO NPs synthesized with IPA solvent have the highest transmittance and band gap energy of 3.3eV. According to DLS data, various content of MEA stabilizer in solvent affects the hydrodynamic size of ZnO NPs.

1. Introduction

The main purpose of research on nanomaterial production methods is to control the composition, size, and shape of NPs. Each of these factors plays a crucial role in establishing the properties of the materials that are used in various technological applications [1,2]. Zinc oxide is a multifunctional material because of its unique physical and chemical features, including high chemical stability, high electrochemical coupling coefficient, a broad spectrum of radiation absorption, and high photostability [3,4]. ZnO has two obvious features that have made it a very important semiconductor. First, at 300 K, it exhibits a direct band gap of 3.4 eV and can create high-quality heterostructures. Second, it was observed that ZnO has an important exciton binding energy of 60 MeV. At room

* Corresponding author.
E-mail address: kazimaria@du.ac.bd (K.H. Maria).

https://doi.org/10.1016/j.heliyon.2023.e20871
Received 17 May 2023; Received in revised form 5 September 2023; Accepted 9 October 2023
Available online 10 October 2023

temperature, this high exciton binding energy can simply translate to much better optical quantum efficiency; potentially resulting in a much lower laser threshold [4]. ZnO is a low-dimensional nanostructure material with unique physio-chemical properties. Being an II-VI compound, it covers a wide variety of infrared and far-infrared applications and also is well recognized in low-voltage and short-wavelength optoelectronics applications due to its wide bandgap, high exciton gain, and substantial exciton binding energy [5–7].

Nowadays the most pressing environmental issue related to global warming and climate change is the rising level of CO_2 concentration from the usage of fossil fuels. Researchers have revealed that using solar energy to photo-catalytically convert CO_2 into hydrocarbons would be the best technique to reduce the atmospheric CO_2 concentration and simultaneously produce sustainable chemical fuels. Researchers have used semiconductor photocatalysts in a pioneering investigation into the reduction of CO_2 [8]. Since then, numerous scientific investigations have focused on creating effective photocatalysts for CO_2 photo reduction [9–14]. ZnO-based nanostructures of various sizes and morphologies have received the most attention as photocatalysts because they are stable, non-toxic, and low-cost [15–18]. However, the CO_2 photoreduction efficiencies of these ZnO-based photocatalysts were often insufficient [19, 20], which could be attributed to the low affinity between CO_2 and ZnO surfaces [21]. Based on these considerations, it was chosen as the initial composition for the current study based on these considerations.

As is well known, CO_2 immobilization can be efficiently assisted by amine functionalization, and this technique has been widely employed in industry to capture CO_2 [22,23]. To encourage CO_2 capture, significant efforts have been undertaken to deposit amine groups onto the surfaces of solid materials [24,25]. When amine groups and CO_2 interact chemically, carbamate (or bicarbonate) is created, which can then be hydrolyzed to produce carbonate [26]. ZnO NPs' optical, chemical, and structural characteristics are influenced by the precursors, solvents, temperature, and time used in their synthesis. It's crucial to investigate the effects of various solvents on the structural, morphological, and optical features of ZnO NPs. Previous research has used isopropyl alcohol (IPA), methanol (MeOH), and 2-methoxyethanol (2-ME) to investigate the effects of various solvents [27]. Few investigations on ethanol (EtOH)–based ZnO thin films have been published [28]. The effect of Monoethanolamine (MEA) content on ZnO thin films was studied by Ahmet Tumbul [29]. It was discovered that the MEA content has a direct effect on the crystalline development orientation of these ZnO thin films [29]. Based on these considerations, MEA has been chosen as a stabilizer for the current study.

Different methods were used to synthesize ZnO NPs [30–34]. The control of physical and chemical features such as size, size dispersity, shape, surface state, crystal structure, organization onto a support, and dispensability is demonstrated in many uses of ZnO NPs [35]. As a result, a wide range of approaches for manufacturing the molecule has been developed. H. R. Ghorbani et al. developed a simple technique to synthesize ZnO nanoparticles. Zinc nitrate and KOH were used in the precipitation of zinc oxide [36]. Researchers have developed a simple precipitation procedure for the manufacture of zinc oxide [37]. For the cost-effective preparation of ZnO NPs, a single-step procedure with large-scale manufacturing without contaminants is preferred [1,38]. Zinc oxide nanoparticles (ZnO NPs) have several limitations that should be considered during synthesis. Their small size and high surface area-to-volume ratio can lead to increased reactivity and potential toxicity. ZnO NPs can undergo chemical transformations or degradation in certain environmental conditions, such as high temperatures, high humidity, or exposure to acidic or basic environments. This can limit their performance and stability in applications where such conditions are present [27–30,37]. ZnO NPs have a high tendency to agglomerate or form clusters due to their high surface energy, leading to decreased surface area and reduced effectiveness in certain applications. This agglomeration can affect their dispersibility and stability in suspensions or matrices. Therefore, achieving precise control over the size and shape during synthesis is challenging.

In this paper, we present a simple technique to manufacture amine-functionalized ZnO NPs by using MEA, which has a hydroxyl (-OH) group for covalent attachment on ZnO and a primary amine ($-NH_2$) group to bestow an amine-functionalized surface. MEA is commonly used as a stabilizing agent for preparing zinc oxide (ZnO) nanoparticles due to its ability to prevent agglomeration and ensure uniform particle size distribution. When preparing ZnO nanoparticles, the particles tend to aggregate or clump together due to the high surface energy of the particles. This can lead to uneven particle size distribution and affect the properties of the resulting nanoparticles. MEA adsorbs onto the surface of the ZnO nanoparticles, creating a steric hindrance that prevents the particles from coming into close contact with one another. This helps to maintain the uniformity of the particle size and prevents agglomeration. The pertinence and novelty of this study lie in the exploration of MEA-stabilized synthesis of ZnO NPs in different solvents and the comprehensive analysis of their structural and optical properties. Understanding how solvent selection and MEA content influence the properties of ZnO NPs can contribute to the development of efficient photocatalytic materials for CO_2 reduction and other technological applications.

2. Experimental

2.1. Sample preparation method

ZnO NPs were synthesized by the simple chemical precipitation method. A ZnO seed solution was made initially to produce ZnO NPs. Zinc acetate dihydrates [Zn $(CH_3COO)_2.2H_2O$] were used as a precursor to prepare the ZnO seed solution. In the process of making ZnO nanopowder, two different synthesis routes named i) water route and ii) alcohol route have been employed. In the water route, 4.3 gm (27.23 mmol) zinc acetate dihydrate [Zn $(CH_3COO)_2.2H_2O$] was dissolved in 100 ml (5555 mmol) water. On the other hand, in the alcohol route, 100 ml (1310 mmol) isopropanol[C_3H_8O] was used as a solvent instead of water. In both routes, the prepared solution was continuously stirred at 60 °C for 30 min by a magnetic stirrer to obtain the most homogenous distribution of elements. Then, exactly the same amount (15 ml or 245 mmol) of Monoethanolamine solution [C_2H_7NO] (MEA) was added drop by drop to the homogeneous solution as a stabilizer in both water and alcohol routes while the solution was continuously stirred at 60 °C

for 2 h. The precursor quantity in both volume and molar quantity is shown in Table 1 below.

Thereafter, a clear and homogeneous solution was created in both water and alcohol routes. After a few days of the aging period, NPs were observed to deposit at the bottom of the beaker. The deposited part was collected by filtering and dried in an oven at 100 °C for 30 min. Throughout the process, the pH level of the solution was found to be between 10.8 and 11.2. Firstly, ZnO NPs were prepared by using Isopropanol and deionized water respectively as solvents keeping the amount of MEA (15 ml) fixed. Then ZnO NPs were prepared by varying the amount of MEA (15 ml, 7.2 ml, and 3.6 ml respectively) in Isopropanol. A schematic diagram of sample preparation is shown in Fig. 1.

2.2. Characterization technique

The crystallographic properties of powder materials, including the lattice parameter (a), crystallite size (D), phase identification, and purity of the calcined powders were carried out using an x-ray diffractometer (Philips X'Pert Pro XRD system operating at 40 kV and 30 mA) with Cu-Kα radiation of wavelength 1.5406 Å was used in the 2θ range of 10–80°. Infrared spectra were recorded in the region of 400–4000 cm^{-1} on an IR Prestige 21, Shimadzu Corporation (Kyoto, Japan). The microstructure of the samples was examined by Scanning Electron Microscopy (SEM) at 20 kV field with 15K and 35K magnification. The grain size was measured from the average of ~40 grains of the corresponding composition using Image J software. To determine the composition of ZnO NPs energy dispersive spectroscopy (EDS) analysis (20 kV and 15K magnification) was carried out. With the help of UV–vis spectroscopy (Shimadzu, 2600), which was used to run over a wavelength range of 400–700 nm, a quartz cuvette with a diameter of 1 cm was used to examine the absorbance spectra of produced NPs solution (ultrasonically dispersed with respective solvents isopropanol and distilled water). The particle size distribution of ZnO NPs was analyzed by DLS using a 633-nm laser and a backscatter measurement angle of 173° (Zetasizer Nano-ZEN 3600, Malvern Instruments, Worcestershire, UK).

3. Results and discussion

3.1. Growth mechanism

The growth mechanism of the powder ZnO NPs involves the hydrolysis, nucleation of monomers to form particles, and growth of particles steps which are represented by the following chemical reaction.

$$Zn(CH_3COO)_2.2H_2O \xrightarrow{C_3H_8O} Zn^{2+} + 2CH_3COO^- + 2H^+ + 2OH^-$$

$$Zn^{2+} + C_2H_7NO \xrightarrow{H_2O} Zn(C_2H_7NO)^{2+} \xrightarrow{H_2O} Zn(OH)_2 + C_2H_7NO + H^+$$

$$CH_3COO^- + 2H^+ + 2OH^- \rightarrow CH_3COOH + H_2O$$

$$Zn(OH)_2 \xrightarrow{\Delta T} ZnO + H_2O$$

Here, isopropanol (C_3H_8O) was used as a solvent for the segregation of zinc acetate dihydrates to release Zn^{2+} ions and acetate ions (CH_3COO^-). MEA (C_2H_7NO) can act as a base and react with Zn^{2+} ions and form a complex compound $Zn(C_2H_7NO)^{2+}$ which undergoes hydrolysis in the presence of water. This hydrolysis reaction leads to the formation of zinc hydroxide ($Zn(OH)_2$), along with a proton (H^+) and releases the MEA. For continuous nucleation, a sufficient amount of OH^- is needed to form $Zn(OH)_2$. After that, the growth of ZnO NPs started from $Zn(OH)_2$ by dissociation. In this process, pH was observed between 10.8 and 11.2 even in the case of aging which also influences the structure and size distribution of the nanoparticles. It's worth noting that the specific mechanism and reaction conditions may vary depending on factors such as temperature, pH, and the molar ratio of reactants. Additionally, the presence of other compounds or additives in the reaction system can influence the reaction pathway and the resulting products. Organic impurities (CH_3COOH) and other unreacted compounds (H_2O) were removed by filtering the solution. As this reaction is endothermic, the heat was supplied to increase the reaction rate which is required for dissociation [39]. Because supplied heat produces more reactant molecules with the required activation energy to enter the reaction and the endothermic reaction rate increases with the increase in temperature.

Table 1
Volume and molar quantity of Precursor used in water and alcohol routes for ZnO nanoparticle synthesis.

Water route	Alcohol route
H_2O	**C_3H_8O (isopropanol)**
100 ml–5555 mmol	100 ml–1310 mmol
Mono Ethanolamine	Mono Ethanolamine
15 ml = 245mmole.	15 ml = 245mmole.
$Zn(CH_3COO)_2.2H_2O$	$Zn(CH_3COO)_2.2H_2O$
4.368 g = 27.23 mmol	4.368 g = 27.23 mmol

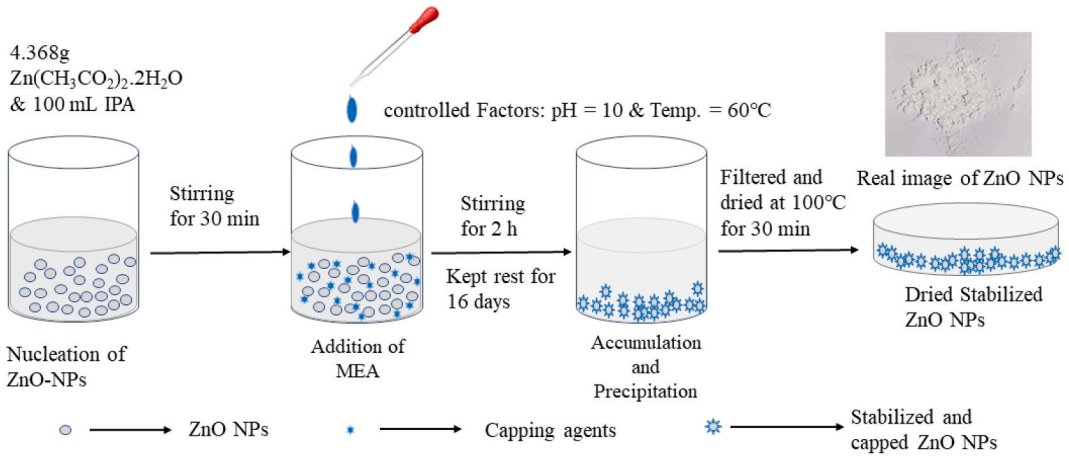

Fig. 1. Schematic diagram of ZnO nanoparticles synthesis via chemical precipitation method.

3.2. X-ray diffraction of the NPs

XRD patterns for ZnO NPs made with two different solvents (isopropanol and deionized water) are shown in Fig. 2(a and b). The sharp and narrow diffraction peaks of the samples affirmed their crystallinity [18,19]. The crystal growth orientation of ZnO NPs displayed their highest peak at different angles for isopropanol and deionized water. While using isopropanol as a solvent, the highest peak was observed at 36.4°, which matches more to the JCPDS 36–1451 reference pattern whereas the highest peak was observed at 33.2° in the case of using deionized water as a solvent.

Although the solution underwent a drying process at 100 °C for 30 min to obtain powder samples, for XRD characterization, it was further annealed at 120 °C for 1 h to investigate possible changes in their crystal structure with increased temperature. Fig. 2(a and b) also show the XRD pattern of annealed ZnO NPs at 120 °C for 1 h in each case. In the case of IPA, the appearance of more sharp and intense peaks than deionized water reveals that IPA as a solvent generates better crystallization without annealing. However, after annealing at 120 °C temperatures, the reduced sharpness of the peak, slightly broad peak, and disappearance of unindexed small peaks have been observed. This peak broadening may be related to the tensile stress and residual non-uniform strain arising in the sample by annealing.

On the other hand, in the case of deionized water, the appearance of more intense peaks and the disappearance of unindexed peaks give a preliminary indication that heating at 120 °C temperatures has led to better crystallization. However, a few extra peaks have appeared by heating and were seen in the XRD pattern which might be for zinc-related secondary and impurity phases [40]. The results indicate that isopropanol is a better solvent than deionized water because IPA didn't show any zinc-related secondary and impurity phases.

XRD patterns for ZnO NPs prepared by isopropanol solvent with different MEA concentrations as stabilizers are shown in Fig. 3(a). To get the more intense peaks, prepared ZnO NPs were heated at 500 °C for 2 h. The hexagonal wurtzite ZnO nanostructure was

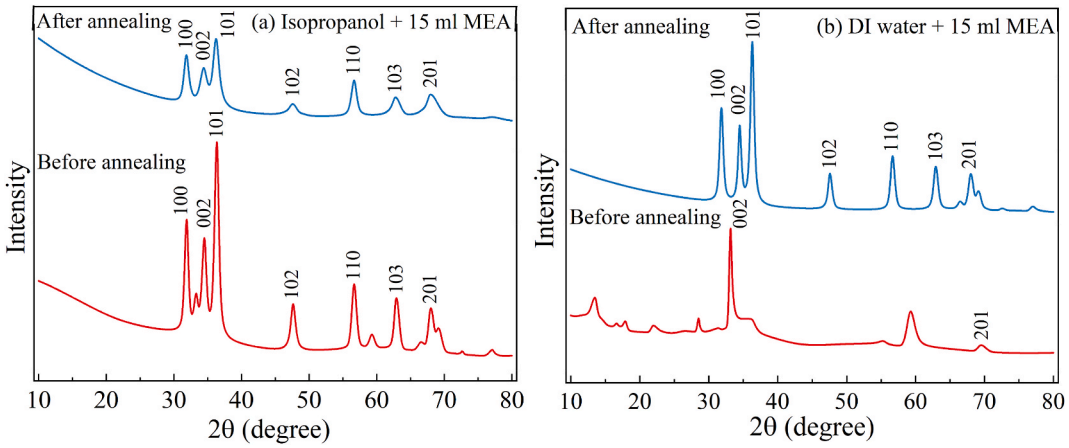

Fig. 2. XRD pattern for ZnO nanoparticles produced by (a) isopropanol + 15 ml MEA (b) deionized water + 15 ml MEA before and after annealing at 120 °C for 1h.

identified by the reflection peaks at (100), (002), (101), (102), (110), (103), (200), (112), and (201). The crystal growth orientation of ZnO NPs exhibits the highest peak at 36.35°, 36.30°, and 36.28° for using 15 ml, 7.2 ml, and 3.6 ml MEA stabilizer respectively. The strong (101) peak indicates that particles have grown along with a preferential orientation owing to small surface energy [20]. No additional peaks were seen in the XRD pattern related to secondary and impurity phases, indicating the high quality of synthesized ZnO NPs. Peak shifting for a different amount of MEA is shown in Fig. 3(b). The peaks are noticed to get shifted towards a smaller value and the full-width half maxima decrease with the decrease in the amounts of MEA. The modest shift in peak position and broadening of the diffraction peaks highlights the effect of MEA on the ZnO lattice and also suggests that changing the quantity of MEA has a substantial effect on the crystal lattice orientation [22]. The smaller value of FWHM indicates that the ZnO particles are more textured along the c-axis [23]. Previous investigations found similar outcomes [21,22].

3.2.1. Lattice constant

The lattice constant of ZnO NPs synthesized by using different solvents was calculated by Cohen's method [38] and is given in Fig. 4. ZnO NPs synthesized by using deionized water possess a smaller lattice constant than those synthesized by using IPA. According to the literature, particle size and lattice constant are closely correlated, with an increase in particle size leading to a proportional decrease in lattice constant [38]. From Fig. 4, the ZnO NPs synthesized by using different amounts of MEA are found to have the unaltered lattice constant which is consistent with previously reported results [24].

3.2.2. Models for analyzing crystallite size

The crystallite size, strain, stress, and deformation energy were calculated by using Debye–Scherer method, uniform deformation model (UDM), Uniform Stress Deformation Model (USDM), uniform deformation energy density model (UDEDM), Size strain plot method (SSP) method. Comparisons of crystallite size, strain, stress, and deformation energy of ZnO NPs synthesized by using deionized water and IPA with different MEA concentrations are listed in Table 2.

The values of average crystallite size obtained from three models of Williamson Hall (W–H) models (i.e. UDM, UDSM, and UDEDM) are almost the same. However, large variations were found in crystallite size calculated from the Scherrer formula and the W–H method. This is due to the difference in averaging the particle size distribution. From all these models, it is seen that ZnO NPs synthesized by using deionized water exhibit increased crystalline size, stress, strain energy, and decreased strain than those synthesized by using IPA as shown in Fig. 5(a).

In the case of MEA concentration variation, the crystalline size of ZnO NPs was found to increase with decreasing the concentration of MEA from 15 ml to 3.6 ml while keeping the concentration of 'IPA' constant as shown in Fig. 5(b). At the same time, the deformation energy of NPs was also increased. The strain was found to be increased and the stress was decreased with a decrease in MEA concentration which is consistent with previously reported results [41]. From Tables 2 and it can also be seen that enhanced heating increased the average crystallite size of ZnO NPs and the crystallite size did not seem to change remarkably with the variation of MEA concentration.

3.3. Fourier-transform infrared spectroscopy analysis

FTIR transmission spectra of ZnO NPs produced by deionized water and isopropanol with different amounts of (MEA) exhibited peaks at the same wavelength region as shown in Fig. 6. The large transmission peak at 3500 cm^{-1} is attributed to the typical polymeric O–H stretching vibration of H_2O in the Zn–O lattice [25], which could be caused by moisture in the solution or in the environment. Another peak at 1562 cm^{-1} is attributed to H–*O*–H bending vibration, which is linked to a minor amount of H_2O in the crystals. The peak observed at 1390 cm^{-1} shows the presence of carbonyl (C═O) groups stretching vibration due to isopropanol and MEA used [42].

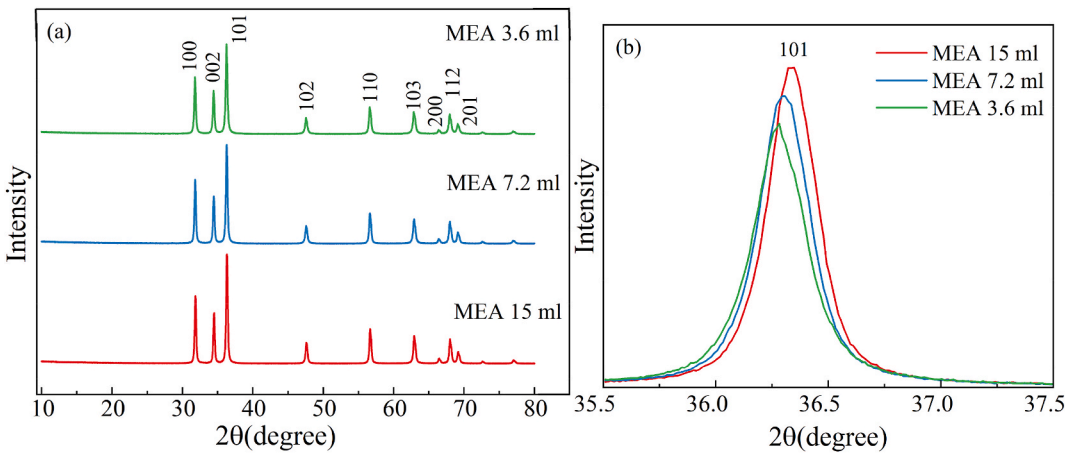

Fig. 3. XRD pattern (a) for ZnO nanoparticles produced by constant isopropanol solvent with various amounts of MEA heated at 500 °C for 2 h. (b) peak shifting for (101) plane.

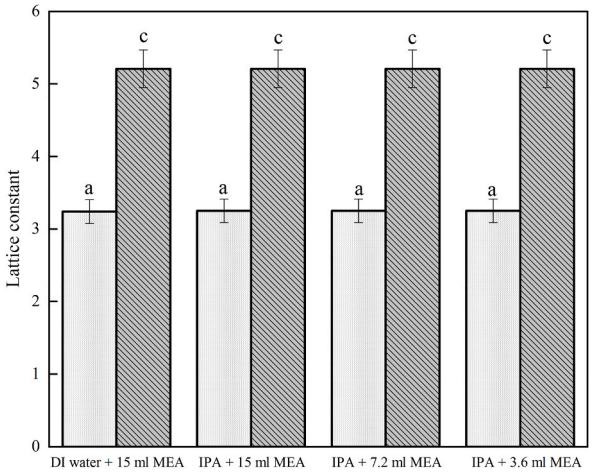

Fig. 4. Comparison of lattice constants of ZnO nanoparticles by varying solvent and stabilizer.

Table 2
Geometric parameters of the ZnO nanoparticles estimates under Debye-Scherrer and three models of Williamson Hall (W–H) (i.e. UDM, USDM, UDEDM, and SSP) methods by using different solvents and various amounts of stabilizer.

Method	ZnO Nanoparticles	Heating Temperatures and Time	Parameter			
			Size (nm)	strain	Stress (MPa)	U (J/m^3)
Debye-Scherrer	DI water + MEA 15 ml	120 °C for 1 h	15.4			
	IPA + MEA 15 ml		8.04			
	IPA + MEA 15 ml	500 °C for 2 h	34.26			
	IPA + MEA 7.2 ml		36.14			
	IPA + MEA 3.6 ml		38.18			
	DI water + MEA 15 ml	120 °C for 1 h	17.24	1.09×10^{-3}		
UDM	IPA + MEA 15 ml		7.8	-4.45×10^{-4}		
	IPA + MEA 15 ml	500 °C for 2 h	46.22	1.14×10^{-3}		
	IPA + MEA 7.2 ml		47.08	9.67×10^{-4}		
	IPA + MEA 3.6 ml		50.54	9.63×10^{-4}		
	DI water + MEA 15 ml	120 °C for 1 h	17.23	8.04×10^{-3}	135.33	
USDM	IPA + MEA 15 ml		7.86	1.76×10^{-2}	44.6	
	IPA + MEA 15 ml	500 °C for 2 h	45.5	1.11×10^{-3}	138.19	
	IPA + MEA 7.2 ml		46.4	9.36×10^{-4}	117	
	IPA + MEA 3.6 ml		49.43	9.23×10^{-4}	115.34	
	DI water + MEA 15 ml	120 °C for 1 h	17.33	8.00×10^{-3}	137	7.50×10^{4}
UDEDM	IPA + MEA 15 ml		7.83	1.77×10^{-2}	51.2	1.05×10^{4}
	IPA + MEA 15 ml	500 °C for 2 h	46.22	1.1×10^{-3}	141.24	7.96×10^{4}
	IPA + MEA 7.2 ml		46.9	9.56×10^{-4}	120	5.72×10^{4}
	IPA + MEA 3.6 ml		49.52	9.47×10^{-4}	119	5.61×10^{4}
	DI water + MEA	120 °C for 1 h	12.89	8.96×10^{-3}		
SSP	IPA + MEA		6.17	1.86×10^{-2}		
	IPA + MEA 15 ml	500 °C for 2 h	35.4	5.6×10^{-3}		
	IPA + MEA 7.2 ml		30.8	4.19×10^{-3}		
	IPA + MEA 3.6 ml		35.91	5.27×10^{-3}		

The Zn–OH stretching vibration is indicated by the peak at 1000 cm^{-1} [42]. The sharp and intense transmission peak at 460 cm^{-1} is attributed to the transmission spectra of Zn–O groups [26].

This transmission peak indicates that all the synthesized ZnO NPs displayed a symmetric stretching mode of hexagonal wurtzite structure [27]. The stretching frequency for the Zn–O bond at 453.2 cm^{-1} for ZnO produced by IPA solvent is shifted to a higher frequency at 474.5 cm^{-1} in the case of using deionized water solvent. Deionized water is lighter than isopropanol, so according to accepted theories of vibrational modes in mixed crystals, deionized water should cause an upward shift of ZnO NPs [28]. This frequency shift towards the higher frequency side reveals the covalent attachment of water to the Zn–O [29].

The spectra of different amounts of MEA confirmed the nature of the covalent attachment of MEA on the ZnO surface in the MEA–ZnO NPs. The C–O stretch and C–N stretch are evident from the peaks at 830 cm^{-1} and 678 cm^{-1} respectively owing to MEA on the ZnO surface [35–37]. Therefore, it is claimed from the spectra that MEA molecules are successfully covalently binding on ZnO surfaces [38]. Moreover, the number of covalent bands for using MEA decreases with the decrease of the amount of MEA (Fig. 6). After annealing at 120 °C for 1hr, the FT-IR spectra of the ZnO NPs produced by different solvents still show most of the signature peaks of

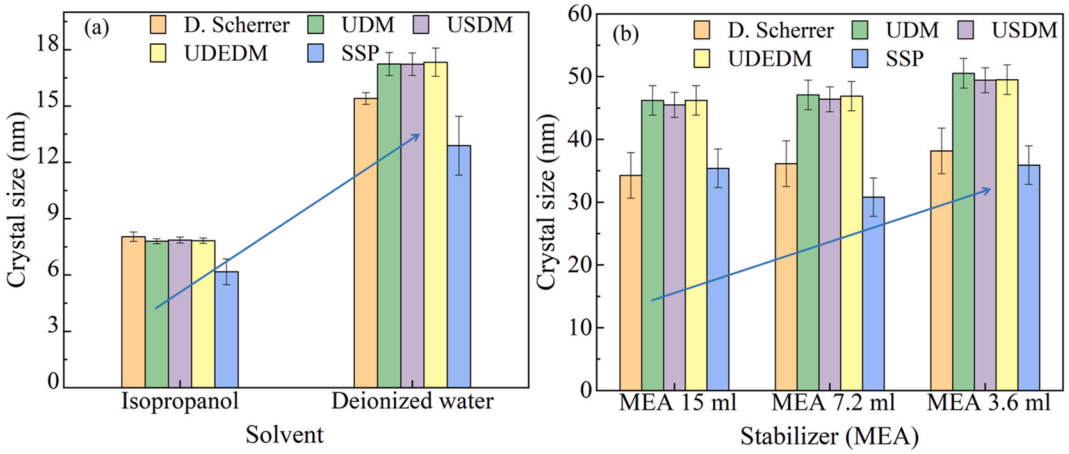

Fig. 5. Crystallite size variation of ZnO nanoparticles synthesized by (a) different solvents and (b) various amounts of stabilizer (MEA).

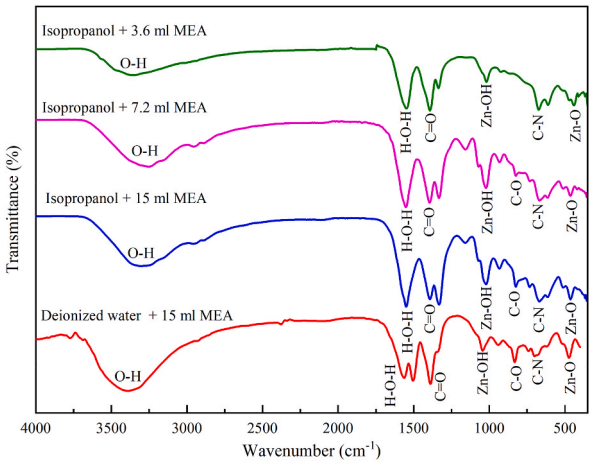

Fig. 6. FTIR transmittance spectra of ZnO nanoparticles with different solvents and various amounts of stabilizer used.

ZnO and MEA, since the boiling point of MEA is ~170 °C [38]. Few peaks of water are absent because the boiling point of water is ~100 °C.

3.4. Scanning Electron Microscopy

Fig. 7(a, c) represent the scanning electron micrographs of water and IPA employing Zinc oxide NPs, respectively which evidently show the different sizes of ZnO NPs prepared in different solvents. In the case of water, ZnO NPs showed a flower-like structure with few spherical crystallites. Approximately the same shape NPs were observed when water was replaced with IPA and the sizes of the synthesized particles are found within the range of 600 nm–800 nm. After annealing at 120 °C for 1 h, the shape of NPs was observed to change from flower-like to spherical with improved crystallinity, and other residual substances got evaporated. Then the size of the spherical-shaped NPs became smaller around 205–400 nm as shown in Fig. 7(c and d).

Fig. 8(a–c) depicts the image of ZnO produced in IPA with different amounts of MEA which shows that the grain size gets smaller with increasing the amount of MEA. It is also observed that the increased amount of MEA also changes the shape of NPs and increases the level of crystallinity. Although the agglomeration of particles was seen on the surface in each case, there were some grains larger than 500 nm in size and some grains were also so tightly packed that it was impossible to determine their size.

The grain size of ZnO NPs using isopropanol as solvent is smaller than the size of ZnO NPs using deionized water as solvent (Fig. 9 (a)). Fig. 9 (b) reveals the grain size of ZnO NPs increases with decreasing the amount of MEA. In general, precipitated ZnO NPs have a porous surface with spherical-shaped nano-sized secondary grains [43]. SEM images also indicate that the microstructures were not entirely homogeneous. Based on the obtained results, it is assumed that the shape and size of the ZnO Nps can be controlled by changing the stabilizer, solvent, aging period, deposition environment, and temperature which affects the morphological qualities.

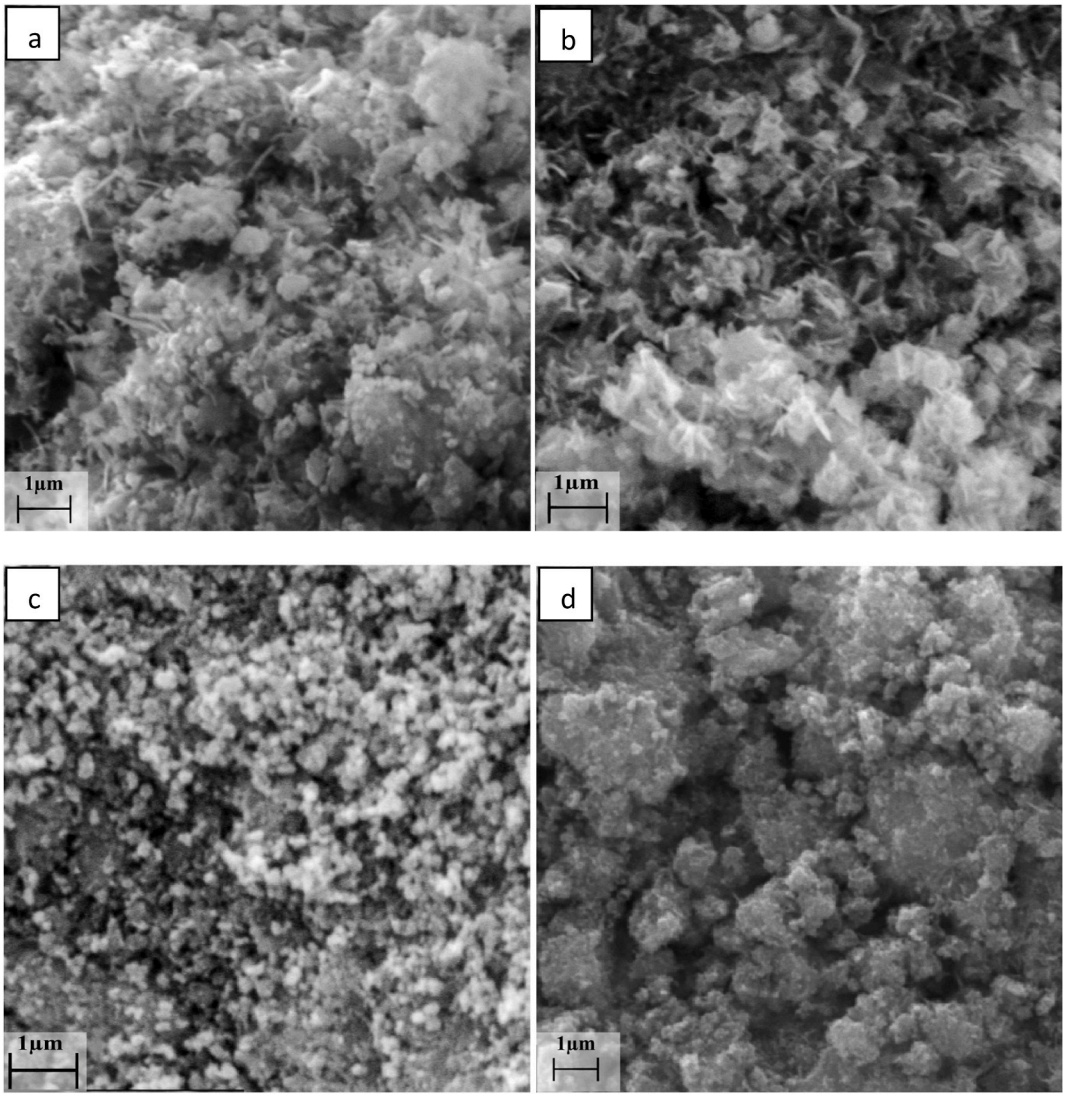

Fig. 7. SEM image at 20 kV field with 15K magnification for ZnO nanoparticles with (a) isopropanol + 15 ml MEA (before heat), (b) deionized water + 15 ml MEA (before heat), (c) isopropanol + 15 ml MEA (after heat), (d) deionized water+ 15 ml MEA (after heat), solvent.

3.5. Energy dispersive spectroscopy

The EDX results of ZnO NPs synthesized by various solvents and stabilizer (Fig. 10) indicate a complete formation and negligible presence of any remnant byproducts (see Fig. 11).

Table 3 shows the elemental analysis of ZnO using EDS. It is found that all four different samples contain excess oxygen. The oxygen atomic percentage was found as 55.98, 61.91, 62.84, and 47.29 while the corresponding Zn atomic percentage was found as 44.02, 38.09, 37.16, and 22.12. The presence of excess oxygen may be due to the presence of some inorganic and organic oxygen species, which were not evaporated during drying samples. It is also observed that, with the decrease of MEA concentration from 15 to 7.2 ml, the oxygen atom percentage was slightly increased from 61.91 to 62.84. This negligible difference in oxygen percentage as a function of MEA concentration is very desirable for the size modification of ZnO NPs by keeping ZnO stoichiometry unchanged as much as possible. However, the sample prepared with 3.6 ml MEA contain carbon atom as carbon peaks appeared in the EDS spectra. Sample with the lowest MEA concentration results agglomeration of ZnO NPs and due to such agglomeration, it is hard to remove or evaporate all the carbon base species from the sample. Similar results were discovered in previous investigations [41]. The theoretical weight percent (%) ratios of Zn and O in ZnO are 80.3 and 19.7 respectively, with atomic percent (%) ratios of 50:50 [44].

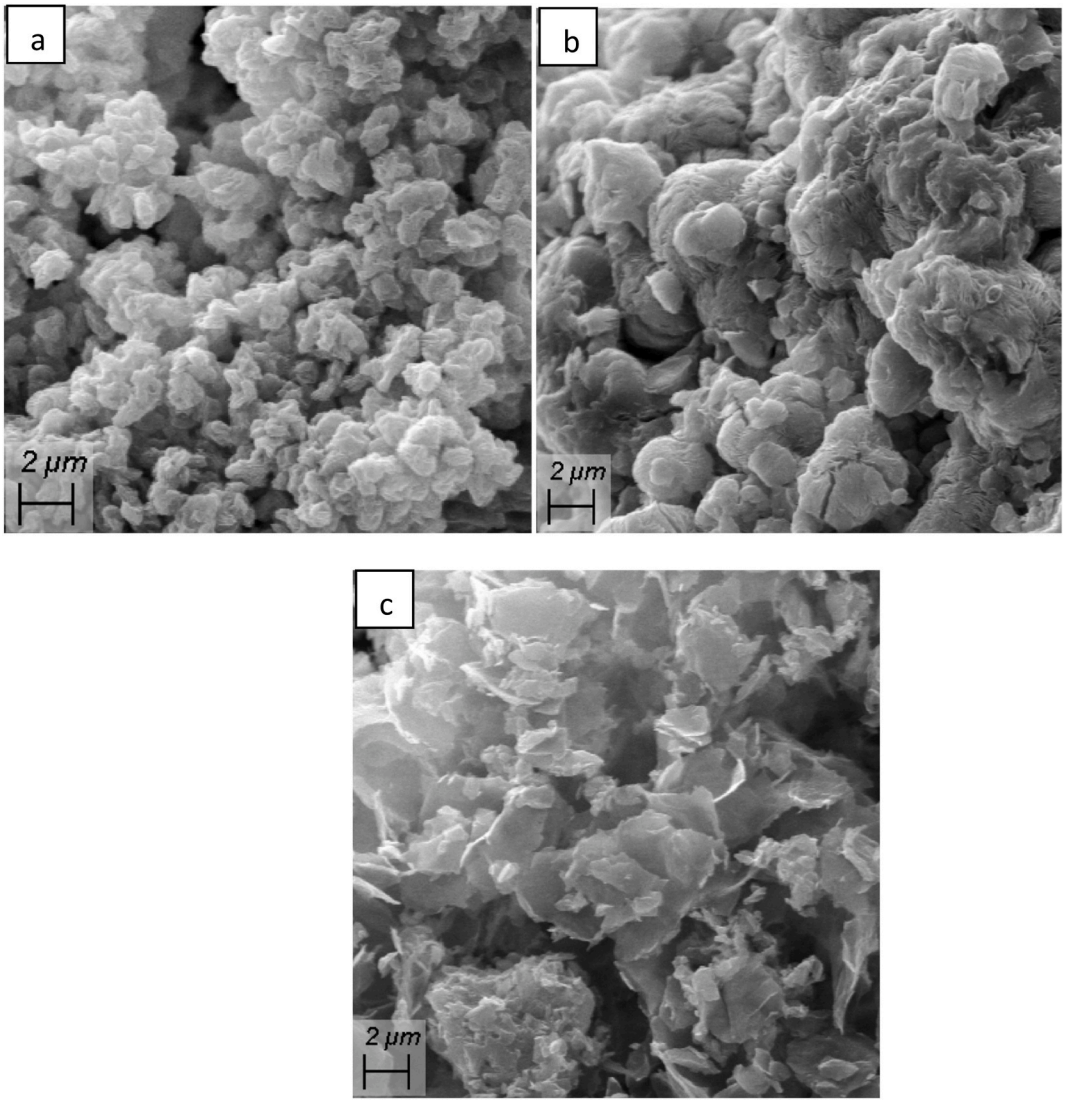

Fig. 8. SEM image at 20 kV field with 15K magnification for ZnO nanoparticles with isopropanol solvent and monoethanolamine (a) 15 ml, (b) 7.2 ml, (c) 3.6 ml.

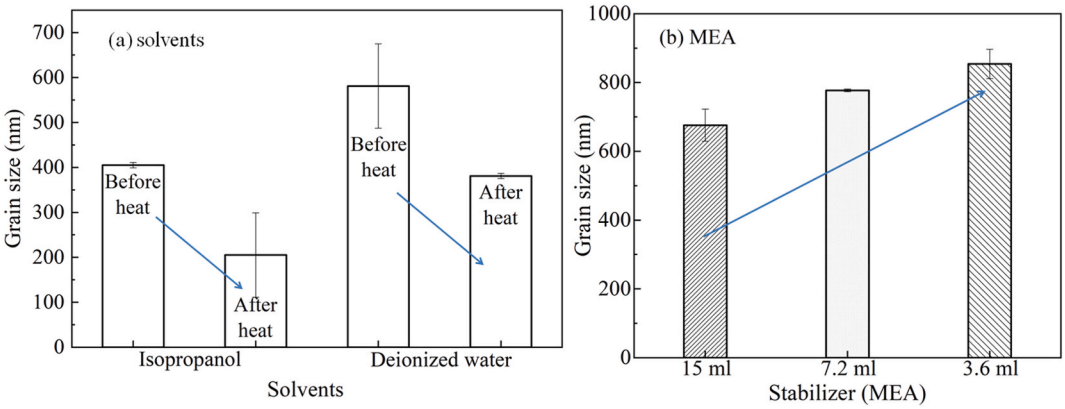

Fig. 9. Variation of grain size with (a) different solvents (b) various amounts of stabilizer (MEA).

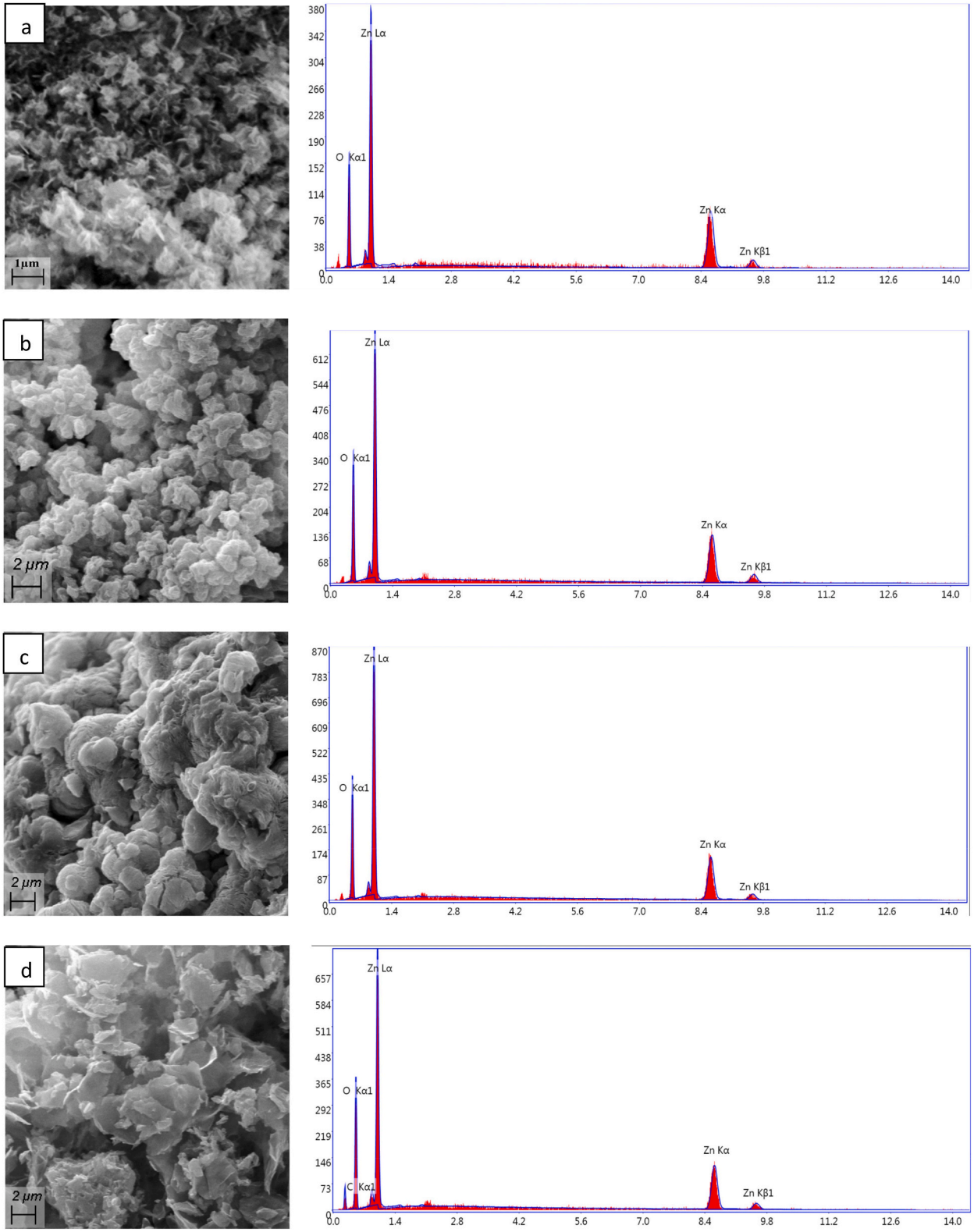

Fig. 10. SEM micrographs at 20kv with 15KX magnification (left) and corresponding EDS spectra (right) for ZnO nanoparticles using (a) deionized water solvent + 15 ml MEA (b) isopropanol solvent + 15 ml MEA (c) isopropanol solvent + 7.2 ml MEA (d) isopropanol solvent + 3.6 ml MEA.

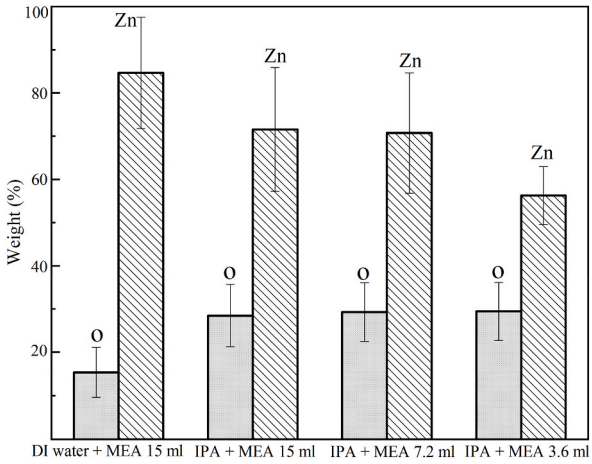

Fig. 11. Comparison of weight (%) of ZnO nanoparticles with different solvents and various amounts of stabilizer (MEA).

Table 3
Atomic and weight percentage of Zn and O from EDS.

ZnO nanoparticles	Element	Weight%	Atomic%
ZnO + DI water	O K	23.73	55.98
	Zn K	76.27	44.02
ZnO + MEA 15 ml	O K	28.46	61.91
	Zn K	71.54	38.09
ZnO + MEA 7.2 ml	O K	29.28	62.84
	Zn K	70.72	37.16
ZnO + MEA 3.6 ml	O K	29.44	47.29
	Zn K	56.26	22.12

3.6. Optical characteristics of NPs

Fig. 12 shows the absorption spectra of the ZnO NPs produced by different solvents and with different MEA in the wavelength range of 100–700 nm. It is seen that the absorbance value is higher from 200 to 390 nm (UV region) and starts decreasing in the region of 400 nm–700 nm (visible region). ZnO NPs produced by isopropanol solvent give an absorbance value of 3.2 % but ZnO produced by deionized water gives an absorbance value of 8.5 %. Therefore, it is conjectured that ZnO NPs produced by isopropanol solvent would be more effective as solar cell window layer than ZnO NPs produced by deionized water [45]. It is observed that different amounts of stabilizer MEA did not affect the absorbance values whereas the absorbance values were changed with different solvents. The

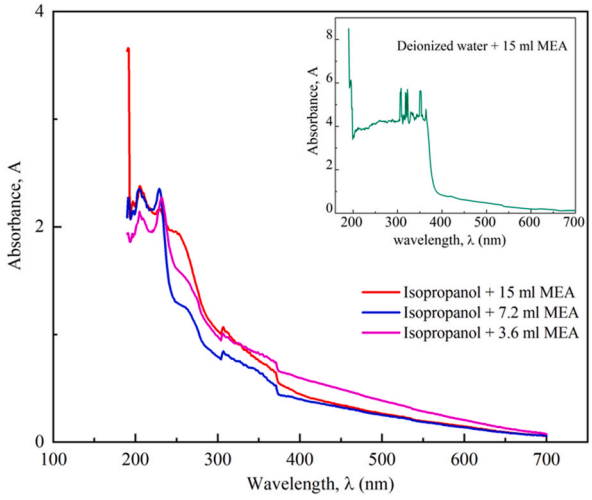

Fig. 12. UV absorbance spectra of ZnO nanopowders produced by different solvents and various amounts of stabilizer (MEA).

absorbance value of ZnO produced by different amounts of MEA is about 2.4 %.

The band gap energy was calculated from the first derivative of the absorbance with respect to photon energy for ZnO produced by different solvents and for ZnO produced by different amounts of MEA as shown in Fig. 13. In both isopropanol and deionized water case, ZnO NPs have the same band gap energy of 3.33 eV. However, the deionized water ZnO NPs shows some extra peaks other than the first peak. In this case, the same band gap energy of 3.33 eV was received from the ZnO NPs regardless of the amount of MEA used, which perfectly matches the theoretical value [46,47]. It is very difficult to differentiate the bandgap in the liquid media since powder samples are homogeneously dispersed in the liquid despite their initial crystallite size in the dry powder form. However, it is important to observe from Fig. 13 that, Isopropanol route shows a clear sharp symmetric line profile with a peak at 3.3eV having no other peaks up to 4 eV.

On the other hand, the sample prepared using a deionized route (Fig. 13 inset) shows comparatively a broader, asymmetric line shape with a peak position at 3.3eV, with other peaks up 4 eV corresponding to chemical species (crystalline or amorphous in nature) prepared during the ZnO preparation in DIA route. It clearly indicates that single-phase ZnO prepared by the IPA route compared to the DIA route has absorption edges in the higher energy regime. The presence of other chemical species surely reduces the electron-hole generation and it will in turn deteriorate the desired optoelectronic properties of the device. The differential spectra provide important information about the optical absorption nature of the powder sample obtained from two different solvents at the same time; it gives further assurance regarding the superior quality of ZnO using an Isopropyl alcohol.

3.7. Dynamic light scattering

The DLS results of Fig. 14 show that the size of NPs varies depending on the solvents and various concentration stabilizers used. The hydrodynamic size distribution was found very broad and inhomogeneous for ZnO NPs synthesized using deionized water as a solvent. The size of the particle varied from 100 nm to as large as 10000 nm with an average hydrodynamic size of 422.2 nm. On the contrary, the size distribution peaks are sharp and homogeneous for ZnO NPs when using IPA as a solvent. The average size of NPs synthesized by using IPA solvent with 15 ml, 7.2 ml, and 3.6 ml MEA is 1697 nm, 1902 nm, and 250 nm respectively.

It is also observed from Fig. 14 that ZnO NPs agglomerates in an aqueous solution. The agglomeration tendency of ZnO NPs has been demonstrated in many pieces of research [48–52]. ZnO NPs were reported to agglomerate in an aqueous solution, but their hydrodynamic size increases with decreasing the amount of MEA. As smaller the hydrodynamic size of NPs, the larger its surface area. Hence it is conjectured that ZnO NPs of smaller hydrodynamic size produced by isopropanol solvent and 3.6 ml MEA would be more effective for drug delivery, heavy metal removal, and many other applications [53].

The purpose of this study was to control the size of NPs by defining the appropriate amount of solvent and stabilizer. A comparative study of our work with previously reported ZnO NPs synthesized by different methods using zinc acetate dihydrates is shown in Table 4. In our study, a small amount of Monoethanolamine (MEA) was used as a stabilizer with zinc acetate dihydrates to prevent agglomeration of NPs and control the size of NPs. From the table, it is clearly observed that the stabilizer can control the size of the synthesized ZnO NPs and exhibit improved optical properties. Therefore, from the above discussion, we conclude that ZnO NPs synthesized by IPA solvent and 15 ml MEA shows smaller crystal-size NPs, homogeneous microstructure, wide band gap energy, and high transmissive property. This result will provide the path for more investigation and extensive optimization of the deposition parameters including growth temperature and deposition time.

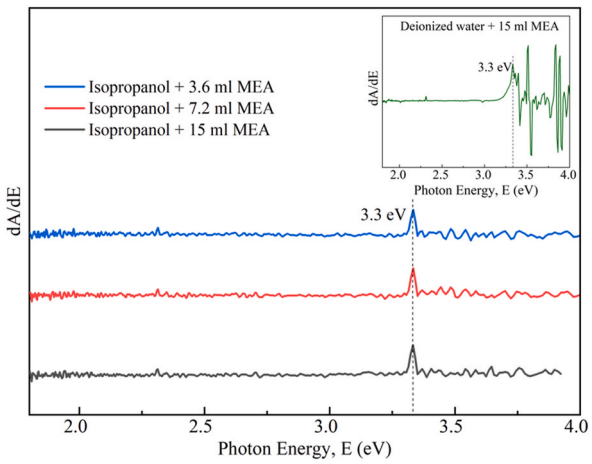

Fig. 13. First derivative of absorbance in terms of photon energy for the ZnO samples synthesized by different solvents and various amounts of stabilizer (MEA).

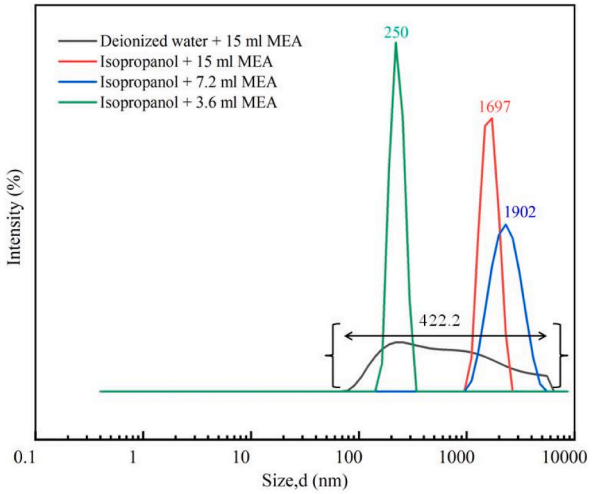

Fig. 14. Particle size variation of ZnO nanoparticles prepared with different solvents and various amounts of stabilizer (MEA).

Table 4
A comparative study of ZnO NPs synthesis by different methods with this work.

Synthesized method		Particle size (nm)	Atomic (%)		Band gap (eV)	Reference
			Zn	O		
Sol-gel		84.98	55.38	44.62	–	30
Ball Milling		13.07	45.15	54.85	3.39	31
Hydrothermal		32.49	–	–	3:29	32
Green Synthesis		26.04	51.38	48.21	3.69	33
Spray-Pyrolysis		14.5	–	–	3.11	34
Chemical precipitation	MEA (15 ml)	34.26	38.09	61.91	3.33	This work
	MEA (7.2 ml)	36.14	37.16	62.84	3.33	
	MEA (3.6 ml)	38.18	22.12	47.29	3.33	

4. Conclusion

In this study, Zinc Oxide (ZnO) NPs have been synthesized successfully by a simple chemical precipitation method. The XRD studies confirm the wurtzite crystal structure and almost the same lattice constant for all ZnO NPs. Physical parameters such as crystalline size, strain, stress, and deformation energy indicate good crystallization for ZnO NPs synthesized by using isopropanol solvent and 15 ml MEA. FTIR spectra demonstrate that the stretching mode of Zn–O bonds moved to a higher frequency state with the decrease in NPs size while using isopropanol as a solvent to synthesize ZnO NPs rather than deionized water. It also verified the nature of the covalent attachment of MEA on the ZnO surface in the MEA–ZnO NPs. Surface morphology reveals that the grain size of ZnO NPs produced by isopropanol as solvent is smaller than that of ZnO NPs produced by using deionized water as solvent. Grain size increases with decreasing concentration of MEA. The EDX results of ZnO NPs synthesized by various solvents indicate a complete formation and negligible presence of any remnant byproducts. From UV vis spectroscopy, it can be commented that 15 ml IPA-ZnO NPs are highly transmissive which is the main condition to be a good window layer of the solar cell. At the same time, the wide bandgap energy of 3.33 eV has been received from all the ZnO NPs. DLS data revealed that ZnO NPs formed agglomerates in an aqueous solution and the size of NPs varies depending on the solvent and stabilizer used.

Author contribution statement

M. Ummay Sumaya: Performed the experiments; Analyzed and interpreted the data, Wrote the paper.
Kazi Hanium Maria: Supervision, Performed the experiments; Analyzed and interpreted the data, Wrote the paper and review.
F. T. Z. Toma: Performed the experiments; Analyzed and interpreted the data.
M. A. Zubair: Performed the experiments; Analyzed and interpreted the data.
M. T. Chowdhury: Supervision, Conceived, and designed the experiments; Performed the experiments; Analyzed and interpreted the data, Contributed reagents, materials, analysis tools, or data. Wrote the paper.

Data availability statement

Data will be made available on request.

Declaration of competing interest

The authors declare the following financial interests/personal relationships which may be considered as potential competing interests:

Kazi Hanium Maria reports administrative support, equipment, drugs, or supplies, and statistical analysis were provided by Department of Physics, University of Dhaka and Experimental Physics Division, Atomic Energy Centre, Dhaka. Kazi Hanium Maria reports a relationship of University of Dhaka with Centre for Advanced Research in Sciences, Bangladesh University of Engineering and Technology, Bangladesh Atomic Energy Centre, Bangladesh Council of Scientific and Industrial Research that includes: non-financial support.

Acknowledgment

The authors are sincerely grateful to Nano, Advanced Materials Laboratory, Department of Physics, University of Dhaka, Experimental Physics Division, Atomic Energy Centre, Dhaka for providing access to experimental facilities. We also thank the Institute of Fuel Research and Development, Bangladesh Council of Scientific and Industrial Research (BCSIR), Centre for Advanced Research of Sciences (CARS), University of Dhaka, and Department of Nanomaterials and Ceramic Engineering, BUET, Dhaka for their co-operation while carrying out this research.

References

[1] A. Edwin Chandross, D. Robert Miller, Nanostructures: Introduction, Chem. Reviews 99 (7) (2009) 1641.
[2] D. Jalali, R. Samson, J. Matsui, H.J. Am, Doughnut-shaped peptide nano-assemblies and their applications as nanoreactors, Chem. Soc. 126 (2014) 7935.
[3] D. Segets, J. Gradl, R. Taylor, K. Vassilev, V. Peukert, Analysis of optical absorbance spectra for the determination of ZnO nanoparticle size distribution, solubility, and surface energy, A. Chem. Society 3 (2019) 1703.
[4] R. Guo, X. Lou, J. Sens, T. Technol, Effective bottom-up synthesis and characterization of nano ZnO particles, JREAS 3 (2009) 1.
[5] R. Wu, Y. Yang, S. Cong, Z. Wu, C. Xie, U. Hiroyuki, K. Kawaguchi, N. Koshizaki, Fractional dimension and photoluminescence of ZnO tetrapod nanowishkers, Chem. Phys. Lett. 406 (2005) 457.
[6] R. Wu, Y. Yang, S. Cong, J. Kong, C. Xie, Optical absorptive characteristics of ZnO tetrapod nanowhiskers, Mater. Lett. 58 (2004) 3792.
[7] W. Zhang, H. Wang, K.S. Wong, Z.K. Tang, G.K.L. Wong, Third-order optical nonlinearity in ZnO micro-crystallite thin films, Appl. Phys. Lett. 75 (1999) 3321.
[8] I. noue, T. Fujishima, A. Konishi, S.K. Honda, Photoelectrocatalytic reduction of carbon dioxide in aqueous suspensions of semiconductor powders, Appl. Phys. Lett. 277 (1979) 637.
[9] C. Wang, O. Ranasingha, S. Natesakhawat, P. Ohodnicki, R. Andio, M. Lewis, J.P. Matranga, C, "Visible light plasmonic heating of Au-ZnO for the catalytic reduction of CO_2", ACS Nano 5 (2013) 6968.
[10] S.C. Roy, O.K. Varghese, M. Paulose, C.A. Grimes, Toward solar fuels: photocatalytic conversion of carbon dioxide to hydrocarbons, ACS Nano 4 (2010) 1259.
[11] J. Highfield, "Advances and recent trends in heterogeneous photo (Electro)-Catalysis for solar fuels and, Chem.",S. Molecules 20 (2015) 6739.
[12] K. Mori, H. Yamashita, M. Anpo, Photocatalytic reduction of CO_2 with H_2O on various titaniumoxide photocatalysts, RSC Adv. 2 (2012) 3165.
[13] W. Fan, Q. Zhang, Y. Wang, Semiconductor-based nanocomposites for photocatalytic H_2 productionand CO_2 conversion, Phys. Chem. Chem. Phys. 15 (2013) 2632.
[14] S. Liu, J. Xia, J. Yu, Amine-functionalized titanate nanosheet-assembled yolkshell microspheres for efficient cocatalyst-free visible-light photocatalytic CO_2 reduction, ACS Appl. Mater. 7 (2015) 8166.
[15] J. Song, S.A. Kulinich, J. Yan, Z. Li, J. He, C. Kan, H. Zeng, Epitaxial ZnO nanowire-onnanoplate structures as efficient and transferable field emitters, Adv. Mater. 25 (2013) 5750.
[16] T. Reimer, I. Paulowicz, R. Röder, S. Kaps, O. Lupan, S. Chemnitz, W. Benecke, C. Ronning, R. Adelung, Y.K. Mishra, Single step integration of ZnO nano- and microneedles in Si trenches by novel flame transport approach: whispering gallery modes and photocatalytic properties, ACS Appl. Mater. 6 (2014) 7806.
[17] Y.M. Mishra, G. Modi, V. Cretu, V. Postica, O. Lupan, T. Reimer, I. Paulowicz, V. Hrkac, W. Benecke, L. Kienle, Direct growth of freestanding ZnO tetrapod networks for multifunctional applications in photocatalysis, UV photodetection, and gas sensing, ACS Appl. Mater. 7 (2015), 14303.
[18] E.S. Jang, J.H. Won, S.J. Hwang, J.H. Choy, J, Fine tuning of the face orientation of ZnO crystals to optimize their photocatalytic activity, Adv. Mater 18 (2006) 3309.
[19] Y. He, Y. Wang, L. Zhang, B. Teng, M. Fan, A high-efficiency conversion of CO_2 to fuel over ZnO/g-C_3N_4 photocatalyst, Appl. Catal., B 168 (2015) 1.
[20] W. Yu, D. Xu, T. Peng, Enhanced photocatalytic activity of g-C_3N_4 for selective CO_2 reduction to CH_3OH via facile coupling of ZnO: a direct Z-scheme mechanism, J. Mater. Chem. A 3 (2015), 19936.
[21] J. Wang, U. Burghaus, Adsorption dynamics of CO_2 on Zn–ZnO(0001): a molecular beam study, J. Chem. Phys. 122 (2005), 044705.
[22] H. Yang, Z. Xu, M. Fan, R. Slimane, A.E. Bland, I. Wright, Progress in carbon dioxide separation and capture: a review, J. Environ. Sci. 20 (2008) 14.
[23] A. Goeppert, M. Czaun, R.B. May, G.K.S. Prakash, G.A. Olah, S.R. Narayanan, Carbon dioxide capture from the air using a polyamine based regenerable solid adsorbent, J. Am. Chem. Soc. 133 (2011), 20164.
[24] G. Qi, Y. Wang, L. Estevez, X. Duan, N. Anako, A.H.A. Park, W. Li, C.W. Jones, E.P. Giannelis, High efficiency nanocomposite sorbents for CO2 capture based on amine-functionalized mesoporous capsules, Energy Environ. Sci. 4 (2011) 444.
[25] G.T. Rochelle, Amine scrubbing for CO2 capture, Sci 325 (2009) 1652.
[26] Y. Liao, S.W. Cao, Y. Yuan, Q. Gu, Z. Zhang, C. Xue, Efficient CO2 capture and photoreduction by amine-functionalized TiO2, Chem. Eur J. 20 (2014), 10220.
[27] P. Samarasekara, U. Wijesinghe, Optical properties of spin-coated Cu doped ZnO nanocomposite films, GESJ Phy 2 (2015) 1512.
[28] C. Xia, F. Wang, C. Hu, Theoretical and experimental studies on electronic structure and optical properties of Cu-doped ZnO, Alloys and Comp. J. 589 (2014) 604.
[29] A. Tumbul, Effect of monoethanolamine content on the crystallinity of ZnO thin films, S. D. U. Journal of Sci. 14 (2019) 155.
[30] J.N. Hasnidawani, H.N. Azlina, H. Norita, N.N. Bonnia, S. Ratim, E.S. Ali, Synthesis of ZnO nanostructures using sol-gel method, Pro. Chem. 19 (2016) 211.
[31] S. Balamurugan, Josny Joy, M. Anto Godwin, S. Selvamani, T.S. Gokul Raja, ZnO nanoparticles obtained by ball milling technique: structural, micro-structure, optical and photo-catalytic properties, Amer. Ins. Of Phy. 1731 (2016), 050121.

[32] R. Shanmugam, L. Priyanka Dwarampudi, N. Nagaprasad, V.L. Nirmal Bhargavi, Bekele bulcha, jule leta tesfaye, degefa anatol and ramaswamy krishnaraj, "synthesis of zinc oxide nanoparticles by hydrothermal methods and spectroscopic investigation of ultraviolet radiation protective properties", Nano J (2021), 8617290.
[33] S. Faisal, H. Jan, S.A. Shah, S. Shah, A. Khan, M.T. Akbar, M. Rizwan, F. Jan, Wajidullah, N. Akhtar, A. Khattak, Suliman Syed, Green synthesis of zinc oxide (ZnO) nanoparticles using aqueous fruit extracts of myristica fragrans: their characterizations and biological and environmental applications, ACS Omega 6 (2021) 9709.
[34] M. Ali, Ghaffarian, hamid reza, saiedi, mahboobeh and sayyad nejad, "synthesis of ZnO nanoparticles by spray pyrolysis method", Iran, J. Chem. Chem. Eng. 1 (2011) 30.
[35] S. Marouf, A. Beniaiche, H. Guessas, A. Azizi, Morphological, structural and optical properties of ZnO thin films deposited by dip coating method, Mate. Research 20 (2017) 88.
[36] H.R. Ghorbani, F.P. Mehr, H. Pazoki, B.M. Rahmani, Synthesis of ZnO nanoparticles by precipitation method, Orent. J. Chem. 31 (2) (2015) 1219.
[37] U. Ozgur, D. Hofstetter, H. Morkoc¸, ZnO devices and applications: a review of current status and future prospects proceedings, IEEE 98 (2010) 1255, 7.
[38] V.N. Morris, R.A. Farrell, A.M. Sexton, M.A. Morris, Lattice constant dependence on particle size for ceria prepared from a citrate sol-gel, Phy. Conf. S.J 26 (2006) 119.
[39] T. Sahoo, M. Kim, M.H. Lee, L.W. Jang, J.W. Jeon, J.S. Kwak, I.Y. Ko, I.H. Lee, Nanocrystalline ZnO thin films by spin coating-pyrolysis method, J. Alloy Compd.", J Lumin. 491 (2000) 308.
[40] K.L. Foon, M. Kashif, U. Hashim, L. WeiWen, Effect of different solvents on the structural and optical properties of zinc oxide thin films for optoelectronic applications, Ceramics Int 40 (2014) 753.
[41] M. Farahmandjou, Effect OF 1, 2- Hexadecadeniol and LiBEt3H superhydride on the size of FePt nanoparticles, Cond. Matt. 40 (2011) 753.
[42] S.M.E. Sepasgozar, S. Mohseni, B. Feizyzadeh, A. Morsali, Green synthesis of zinc oxide and copper oxide nanoparticles using Achillea Nobilis extract and evaluating their antioxidant and antibacterial properties, Mate. Sci. 44 (2) (2021) 1.
[43] O. Lupan, T. Pauporte, Electrodeposition of Cu-doped ZnO nanowire arrays and heterojunction formation with p-GaN for color tunable light emitting diode applications, Electro. Acta. 56 (2011), 10543.
[44] D. Chakroborti, S. Muthukumaran, R. Gopalakrishnan, Structural, FTIR and photoluminescence studies of Cu doped ZnONPs by co-precipitation method, Appl. Phys. Lett. 90 (2007), 062504.
[45] D. Balzar, H. Ledbetter, Voigt-function modeling in Fourier analysis of size-and strain-broadened X-ray diffraction peaks, J. Appl. Crystal. 26 (1993) 97.
[46] F.K. Shan, Y.S. Yu, Band gap energy of pure and Al-doped ZnO thin films, Eu. ceramic soci. 24 (6) (2004) 1869.
[47] A. Escobedo Morales, E. Sanchez Mora, U. Pal, Use of diffuse reflectance spectroscopy for optical characterization of un-supported nanostructures, Re. Mexi. de Física 53 (5) (2007) 18.
[48] R. Wu, Y. Yang, S. Cong, Z. Wu, C. Xie, H. Usui, K. Kawaguchi, N. Koshizaki, Fractional dimension, and photoluminescence of ZnO tetrapod nanowhiskers, IOP Conf. Ser.: Mater. Sci. 73 (2015), 01213.
[49] Z. Zhang, J.B. Yi, J. Ding, L.M. Wong, H.L. Seng, S.J. Wang, J.G. Tao, G.P. Li, G.Z. Xing, T.C. Sum, C.H. Alfred Huan, T. Wu, Cu-doped ZnO nanoneedles and nano nails: morphological evolution and physical properties, Phy. Chem. J. 112 (2008) 9579. C.
[50] F. Fiévet, R. Brayner, The polyol process. NPs: a danger or a promise, Spri. London 45 (2013) 54.
[51] R. Yogamalar, R. Srinivasan, A. Vinu, K. Ariga, A.C. Bose, X-ray peak broadening analysis in ZnO NPs, Solid State Commun. 149 (2009) 1919.
[52] A.K. Zak, W.H.A. Majid, M.E. Abrishami, R. Yousefi, X-ray analysis of ZnO NPs by Williamson-Hall and size-strain plot methods, Solid State Sci. 13 (2011) 251.
[53] J. Kang Lim, S. Pin Yeap, H. Xin Che, S. Chun Low, Characterization of magnetic nanoparticle by dynamic light scattering, Nano. Res. Lett. 8 (2013) 381.